Applied Physics Letters

RESEARCH ARTICLE | AUGUST 22 2022

Mechanisms for undesired nucleation on H-terminated Si and dimethylamino-trimethylsilane passivated SiO_2 during TiO_2 area-selective atomic layer deposition

Rachel A. Nye; Seung Keun Song; Kaat Van Dongen; ... et. al

Appl. Phys. Lett. 121, 082102 (2022)
https://doi.org/10.1063/5.0106132

CrossMark

View Online

Export Citation

Articles You May Be Interested In

Microloading effect in ultrafine SiO 2 hole/trench etching

Journal of Vacuum Science & Technology A (July 1999)

Electron-stimulated and thermal desorption study of trimethylsilane from Si(100)

Journal of Vacuum Science & Technology A (July 1994)

Study of electron-beam effects on trimethylsilane covered Si(100)

Journal of Vacuum Science & Technology A (November 1995)

Downloaded from http://pubs.aip.org/aip/apl/article-pdf/doi/10.1063/5.0106132/16482657/082102_1_online.pdf

Applied Physics Letters ARTICLE scitation.org/journal/apl

Mechanisms for undesired nucleation on H-terminated Si and dimethylamino-trimethylsilane passivated SiO_2 during TiO_2 area-selective atomic layer deposition

Cite as: Appl. Phys. Lett. **121**, 082102 (2022); doi: 10.1063/5.0106132
Submitted: 27 June 2022 · Accepted: 3 August 2022 ·
Published Online: 22 August 2022

Rachel A. Nye,[1,2,3] Seung Keun Song,[1] Kaat Van Dongen,[2,3] Annelies Delabie,[2,3,a)] and Gregory N. Parsons[1,a)]

AFFILIATIONS

[1]Department of Chemical and Biomolecular Engineering, North Carolina State University, Raleigh, North Carolina 27695, USA
[2]Department of Chemistry, University of Leuven, Leuven B-3001, Belgium
[3]IMEC, Leuven B-3001, Belgium

[a)]Authors to whom correspondence should be addressed: Annelies.Delabie@imec.be and gnp@ncsu.edu

ABSTRACT

During TiO_2 atomic layer deposition (ALD) using $TiCl_4$ and H_2O at ~150 °C, nucleation proceeds rapidly on hydroxylated SiO_2 but is inherently delayed on passivated surfaces such as H-terminated silicon (Si-H) and trimethylsilyl-passivated SiO_2 (SiO_2-TMS) formed using dimethylamino-trimethylsilane (DMA-TMS) as a small molecule inhibitor. In this work, we explore details of TiO_2 nucleation on both Si-H and SiO_2-TMS and show that the mechanisms leading to unwanted nuclei depend strongly on the passivation mechanism. Initial growth is observed as a function of ALD cycles using scanning electron microscopy to obtain average particle size, density, and overall surface coverage fraction. Also, average film thickness vs cycle is estimated using ellipsometry or Rutherford backscattering spectrometry. Data are compared to an analytical model that considers that either nucleation sites are present on the starting non-growth surface or sites are generated during the ALD process. On the Si-H surface, data and modeling indicate that nucleation occurs predominantly from a fixed number of nucleation sites present on the starting growth surface that start to immediately grow. However, on TMS-passivated SiO_2, nucleation sites are predominantly generated during the growth process so that the density of nucleation sites increases as growth proceeds. Results indicate that nucleation sites are created when adsorbed ALD reactants become kinetically trapped on the SiO_2-TMS surface. This demonstrates that mechanisms associated with unwanted nucleation during area-selective deposition (ASD) can depend on details of the surface passivation scheme, thereby providing insight to help to improve ASD strategies for advanced applications.

Published under an exclusive license by AIP Publishing. https://doi.org/10.1063/5.0106132

Low temperature area-selective deposition (ASD) is a promising bottom-up technique to promote nanopatterning for next-generation, sub-10 nm semiconductor manufacturing while complementing or reducing requirements for expensive lithography steps.[1–3] In an ASD process, chemical differences on a patterned substrate are exploited to deposit material on a desired "growth" region, with an adjacent, "non-growth" region selected or designed to inhibit growth.[4,5] For example, during TiO_2 atomic layer deposition (ALD) using $TiCl_4$ and H_2O at ~170 °C, film growth proceeds linearly from the first cycle on hydroxylated SiO_2, while under the same ALD conditions, TiO_2 nucleation is inherently inhibited on H-terminated silicon (Si-H) surfaces.[6] TiO_2 ALD is also inhibited on hydroxylated SiO_2 by reacting surface Si-OH groups with dimethylamino-trimethylsilane (DMA-TMS), forming non-reactive trimethylsilyl surface groups.[7] Formation of the trimethylsilyl-passivated SiO_2, referred to here as SiO_2-TMS, likely proceeds by DMA-TMS physisorption via hydrogen-bonding between the dimethylamino group and surface −OH groups, followed by insertion of a TMS group.[8–11] This process appears to be more facile on Si-OH vs Ti-OH, which may be associated with differences in H-bonding of the hydroxyl groups on each surface.[12,13] In general, using any surface passivation method, continued exposure to the deposition reactants eventually produces unwanted nuclei in the non-growth region.[14] Thus, understanding nucleation and initial growth evolution, especially in the non-growth area, is essential to attain improved

Published under an exclusive license by AIP Publishing

This article may be downloaded for personal user only. Any other use requires prior permission of the author and AIP Publishing. This article appeared in: Rachel A. Nye, Seung Keun Song, Kaat Van Dongen, Annelies Delabie, Gregory N. Parsons; Mechanisms for undesired nucleation on H-terminated Si and dimethylamino-trimethylsilane passivated SiO2 during TiO2 area-selective atomic layer deposition. Appl. Phys. Lett. 22 August 2022; 121 (8): 082102. and may be found at : https://doi.org/10.1063/5.0106132

Downloaded from http://pubs.aip.org/aip/apl/article-pdf/doi/10.1063/5.0106132/16482657/082102_1_online.pdf

selectivity. While several recent studies have utilized fundamental understanding to improve processes,[15–20] the underlying mechanisms that give rise to unwanted nucleation remain unclear.

Herein we demonstrate a general approach to expand understanding of nucleation mechanisms by directly comparing initial nucleation and growth of TiO_2 on clean silicon passivated by hydrogen (Si-H) and by DMA-TMS (SiO_2-TMS). For these two different passivated surfaces, scanning electron microscopy (SEM) is used to quantify the number, surface coverage, and radius size distribution of TiO_2 particles as a function of the ALD cycle. Ellipsometry or Rutherford backscattering spectrometry (RBS) is also used to obtain average film thickness vs ALD cycle. Then, using the thickness per cycle measured on a receptive oxidized silicon surface, $\dot{G}$ (nm/cycle), the measured nucleus radius is compared to the characteristic radius, $r_n = \dot{G} \cdot n$, defined as the radius of a hemispherical nucleus after n cycles under conditions where growth begins immediately at an isolated site and proceeds uniformly in all directions at a rate of $\dot{G}$ nm/cycle. Furthermore, observed nucleus surface coverage and density vs ALD cycle are analyzed by fitting the data to an analytical model for nucleus formation and growth evolution.[14]

In this analysis, nucleation sites are defined as fixed dimensionless points on a surface that are receptive to film growth. If a nucleation site is present, then the model assumes that a physical hemispherical nucleus forms at that site and grows with radius (and nucleus height) $r_n = \dot{G} \cdot n$ (nm). Nuclei coalescence is then modeled using the Avrami equation, an approach to quantify nucleus growth as a function of time that has been previously demonstrated to describe initial ALD growth.[5,14,21] The expected average film thickness vs ALD cycle is attained by integrating the volume of the resulting isolated and coalesced nuclei. In the model, nucleation sites may be present on the starting surface, $\hat{N}$ (nm^{-2}), (i.e., accessible hydroxyl groups or other impurities), and/or generated during the deposition, $\dot{N}$ (nm^{-2} cycle^{-1}), as illustrated in Scheme 1.[5,14] The model also allows for site generation to begin immediately with deposition, or after a characteristic delay period, τ_d (cycles). The model output provides a unique method to quantify differences in nucleation mechanisms on different growth surfaces. We show that this approach can provide direct insight into the nature of unwanted nucleation and could help to develop strategies to reduce unwanted growth during ASD.

For the deposition experiments, small silicon coupons (1.5 $\times$ 1.5 cm^2) with 100 nm of thermally grown SiO_2 are cleaned by dipping in the piranha solution (H_2O_2:H_2SO_4 = 1:1 volume ratio) for 15 min and rinsing with de-ionized water.[6] SiO_2 is also prepared as 17 nm thick films by plasma-enhanced ALD (PEALD) using a silicon precursor and oxygen plasma at 75 °C on 300 mm diameter (100) silicon wafers in an Eagle12 reactor.[16] We note that the different preparation of each growth surface could have some effect on initial nucleation. Some of the PEALD SiO_2 films are directly transferred to a Tokyo Electron Ltd LK-R chamber (Tactras platform) where they are exposed to 300 s of DMA-TMS at 250 °C and 5 Torr in a N_2 environment.[12,22] The relatively higher processing temperature of DMA-TMS exposure [compared to ALD and hydrogen fluoride (HF) dip] must be considered when using thermally sensitive materials. Surfaces are characterized with x-ray photoelectron spectroscopy (XPS, Quantes, 65° incidence angle at 1486.6 eV monochromatized Al K α x-ray source) and water contact angle measurements (WCAs, Dataphysics OCAH 230 tool with 1 μL DI H_2O droplets). After DMA-TMS passivation, XPS results support the presence of Si-$(CH_3)_3$ groups (Fig. S1 and Table SI), and WCA data (Fig. S2) show $\sim$102° consistent with the hydrophobic TMS groups, as compared to more hydrophilic Si-H ($\sim$70°)[6] and SiO_2 ($\sim$25°).[7] For ellipsometry, the Si-H surfaces are prepared as coupons by cleaning silicon in piranha solution to create a

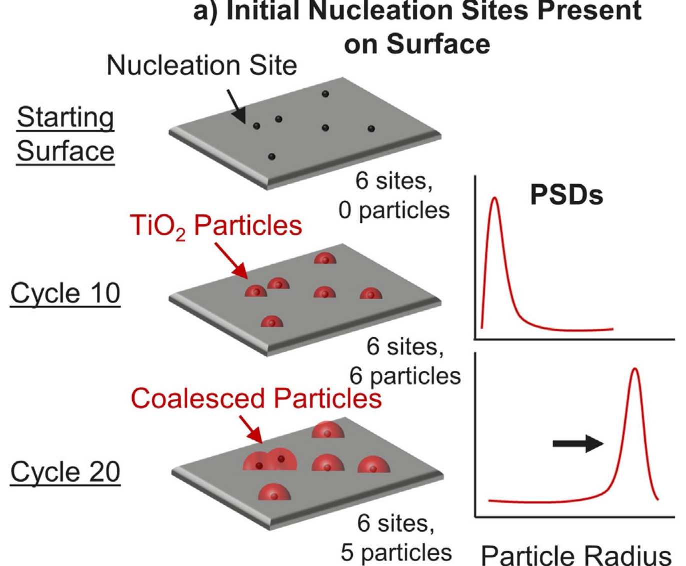

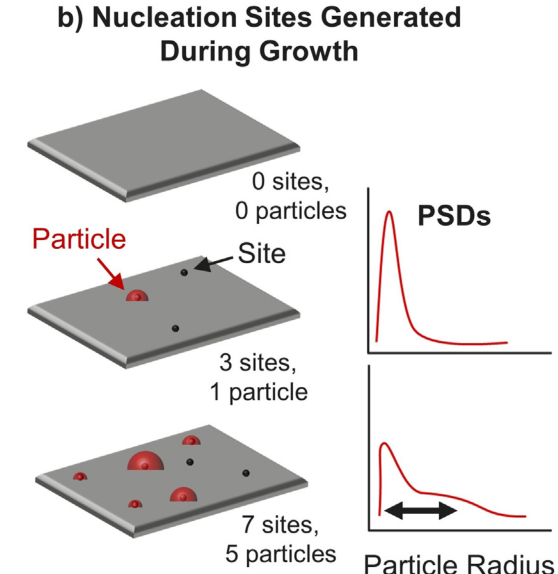

SCHEME 1. Schematic of different nuclei growth scenarios and resulting particle size distributions (PDSs). (a) Nucleation sites (as defined in the text) are initially present on the surface before deposition, and physical nuclei form only on these fixed nucleation sites, resulting in particles of similar sizes that grow with the increase in ALD cycle. (b) The initial substrate surface contains no nucleation sites, and nucleation sites are generated during deposition. Nuclei start to grow on nucleation sites immediately after sites are generated, resulting in a wide range of particle sizes and a high concentration of small particles. Nucleation sites are depicted as black circles, while TiO_2 particles are shown in red.

Downloaded from http://pubs.aip.org/aip/apl/article-pdf/doi/10.1063/5.0106132/16482657/082102_1_online.pdf

Published under an exclusive license by AIP Publishing

chemical oxide, followed by dipping into a 5% aqueous HF solution for 30 s, washing in de-ionized water for 30 s, and drying with flowing N_2. For SEM imaging, Si-H surfaces were prepared by lithographic wet-etching of 100 nm of thermally oxidized silicon followed by the same HF rinse and dry steps.

On each surface, TiO_2 ALD is performed using $TiCl_4$ and H_2O either in a Polygon 8300 EmerALD reactor (for the 300 mm wafers) at 150 °C and 5 Torr N_2[12,13] or in a lab-built tubular flow reactor at 170 °C and 900 mTorr (for the coupon samples).[6] In the Polygon 8300 tool, the effects of purge time and initial degas time on Ti content are analyzed after 100 cycles on SiO_2-TMS. In some experiments on SiO_2-TMS, the DMA-TMS passivation step is repeated periodically every 50 ALD cycles.

After ALD, nuclei formed during the first 200–300 cycles are imaged by SEM using either a FEI Helios 460 (3 kV beam energy, 0.10 nA current) or Verios 460L (10 kV, 0.40 nA) microscope. Average particle size, density, and surface coverage are determined using ImageJ software. Surfaces are also characterized with RBS (1.523 MeV He^+ incoming ion beam, 170° scattering angle, 11° tilt angle, and 20 nA current) and total x-ray fluorescence (TXRF, Rigaku TXRF300 with a 35 kV, 255 mA x-ray beam) to quantify the Ti content, or spectroscopic ellipsometry (J.A. Woollam alpha-SE). The RBS results are converted to an equivalent film thickness using a TiO_2 film density of 3.72 g/cm^3.

Figures 1(a) and 1(b) show SEM images of the Si-H and SiO_2-TMS surfaces, respectively, after various numbers of ALD cycles. Resulting selectivity to each passivated surface is calculated based on surface coverage and plotted in Fig. S3. On the Si-H surfaces, particles with diameter of ∼1–2 nm are observed after 30 cycles, and they increase in size as growth proceeds. After ∼100 cycles, particles appear to be coalesced. On the DMA-TMS passivated surfaces, no particles are observed after 20 and 50 cycles, with some small (∼1–2 nm), isolated particles visible after 75 cycles. Some coalescence is apparent after 100 cycles.

Figures 2(a) and 2(b) show the particle size distributions (PSDs) obtained from the SEM images in Fig. 1 and the corresponding values

Downloaded from http://pubs.aip.org/aip/apl/article-pdf/doi/10.1063/5.0106132/16482657/082102_1_online.pdf

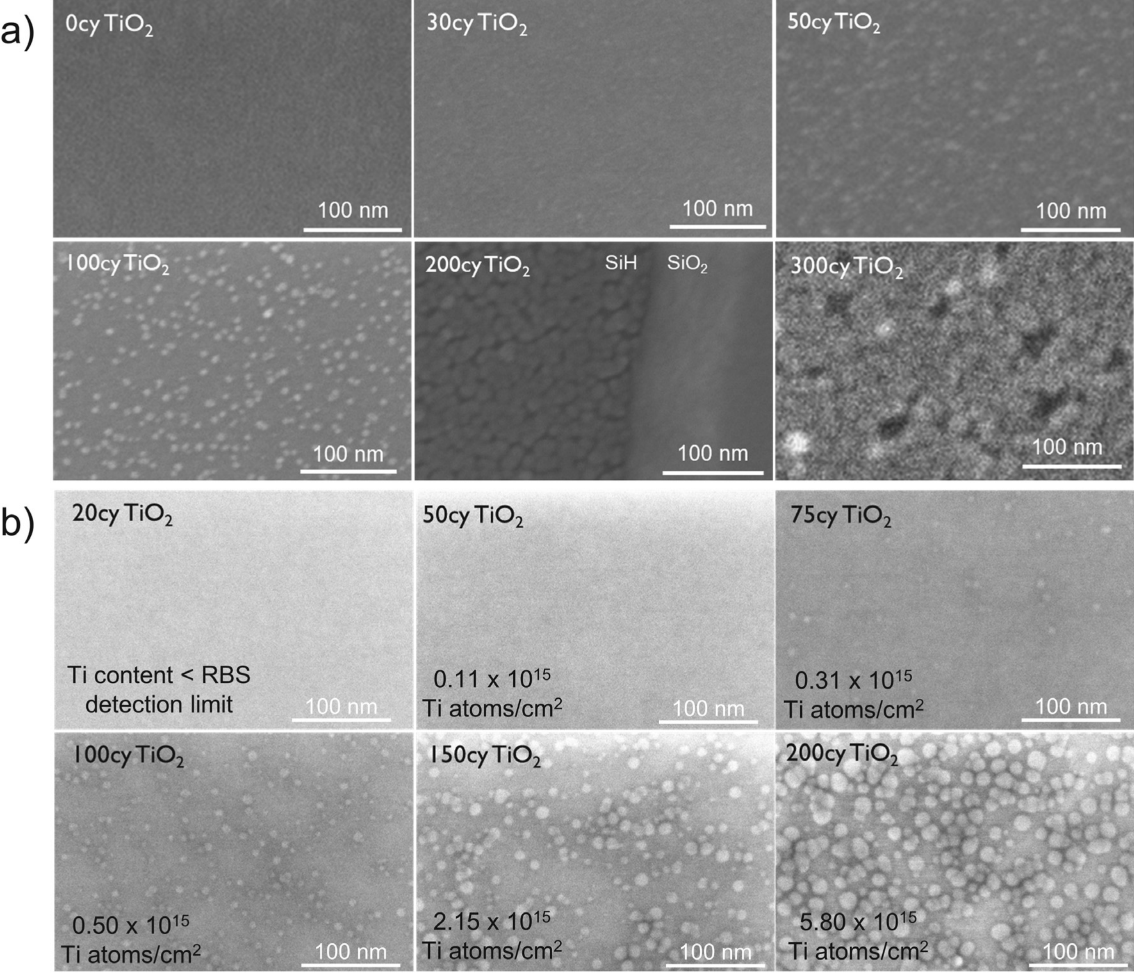

FIG. 1. SEM images of various cycles of TiO_2 (a) deposited at 170 °C on trench patterned Si-H/SiO_2 surfaces and (b) deposited at 150 °C on SiO_2-TMS surfaces. Ti content from RBS is shown in the bottom left corner of (b). Images in (a) are brightened after ImageJ analysis to enhance visual acuity.

Published under an exclusive license by AIP Publishing

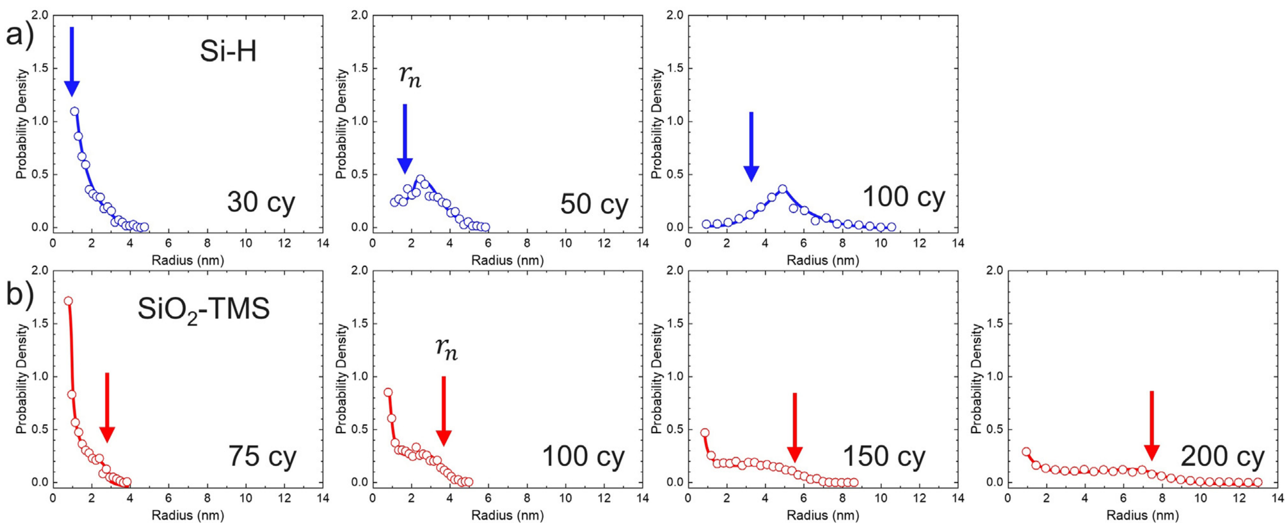

FIG. 2. Particle size distributions (from SEM) for various TiO_2 cycles deposited on (a) patterned Si-H at 170 °C and (b) SiO_2-TMS at 150 °C. Maximum expected height for hemispherical particles grown from cycle 1, i.e., r_n, are indicated by arrows for each sample. Lines are drawn as guides to the eye.

for r_n (defined above). On Si-H [Fig. 2(a)], there is a high concentration of small particles after 30 cycles. As growth proceeds, the density of small particles decreases and the position of the peak shifts to a larger average particle size. On the Si-H surface, the PSD peak radius exceeds r_n, indicating either: (1) some particle coalescence has occurred (i.e., some small nuclei start close together and merge early during the process); and/or (2) the rate of growth in the lateral direction exceeds that in the vertical direction (i.e., the nuclei are not hemispherical). Current analysis and results do not allow us to distinguish these possibilities. Diffusion of nuclei could also affect these results, but substantial diffusion of covalently bound nuclei is not expected at the low growth temperature. Further modifications to the model used here, or a more complex model, such as kinetic Monte Carlo simulations, merit further investigation to describe particle nucleation and growth on non-growth surfaces during ASD.

On SiO_2-TMS [Fig. 2(b)], the PSD results are markedly different from those observed on Si-H. First, for each sample analyzed, there is a relatively large density of small particles. The peak in the PSD is less pronounced and occurs at a value that is smaller than r_n. This trend is consistent with particles that start to grow after some delay period, i.e., the receptive nucleation sites are not present on the starting surface but are generated during the growth process. The different trends in nucleation and their expected influence on the measured PSDs are shown in Scheme 1 and are discussed in more detail below.

The trend in particle size and distribution is consistent with images collected by atomic force microscopy (AFM, Bruker Dimension Edge, 300 kHz tip), shown in Fig. S4. Furthermore, PSDs from SEM images collected after TiO_2 ALD at 300 °C on SiO_2-TMS (Fig. S5) show trends consistent with those in Fig. 2(b) for ALD at 150 °C.

Figures 3 and S7 show results of thickness vs cycle for the various surfaces studied. Figure 3 also shows particle surface coverage and number density from SEM plotted vs ALD cycle. On SiO_2, the growth per cycle in Figs. 3(a) and 3(b) is linear with $\dot{G} = 0.033$ and 0.037 nm/cycle, respectively.[6,13] On Si-H, TiO_2 shows inhibited nucleation, with particles detected by ellipsometry after 30 cycles. TiO_2 ALD is also impeded on the SiO_2-TMS surface, with a small amount of Ti (4.29×10^{12} at/cm^2) detected from TXRF after a single cycle. The trends in surface coverage [Figs. 3(c) and 3(d)] and particle density [Figs. 3(e) and 3(f)] are also distinct on each surface, with a faster increase in surface coverage and more constant particle density on Si-H compared to SiO_2-TMS.

The solid and dashed lines in Fig. 3 correspond to fits to a nucleation and growth model.[5,14] For both starting surfaces in Fig. 3, the measured value of $\dot{G}$ (0.033 or 0.037 nm cycle^{-1}) is input to the model and the value for $\hat{N}$ is adjusted while keeping $\dot{N} = 0$ to obtain a good match with measured average thickness vs cycle, surface coverage, and particle density on each inhibited surface (shown as the set of solid lines in Fig. 3). Importantly, we note that this fit is obtained by adjusting only one parameter, $\hat{N}$, to simultaneously fit three sets of data (thickness, surface coverage, and particle density) obtained independently from two separate measurements (thickness and SEM analysis). To compare different nucleation mechanisms, the fitting process is repeated, in this case by adjusting two parameters: $\dot{N}$ and τ_d, with $\hat{N} = 0$ to obtain a second fit (dashed lines in Fig. 3). Fit parameters for each are given in the figure caption. For simplicity, we choose to compare models by adjusting $\hat{N}$ or $\dot{N}$ individually. Both $\hat{N}$ and $\dot{N}$ could be adjusted simultaneously, but more data points would be needed for a unique fit.

For the fit on the Si-H surface in Fig. 3(a), the solid line, i.e., nucleation sites present on the starting surface ($\hat{N} > 0$; $\dot{N} = 0$), provides an overall better fit than the dashed line for nucleation site generation ($\hat{N} = 0$; $\dot{N} > 0$). For the surface coverage in Fig. 3(c), the solid and dashed lines both show a good fit up to 100 cycles, with the dashed line showing a better fit to the point at 200 cycles. However, for the particle density data, shown in a log scale in Fig. 3(e), the solid line fit ($\hat{N} > 0$) is more representative, particularly up to 100 cycles. We note that it is reasonable for the number of particles observed to be less than the number of physical nuclei because even for small coverage, some nuclei may coalesce, reducing the number of particles

Published under an exclusive license by AIP Publishing

Downloaded from http://pubs.aip.org/aip/apl/article-pdf/doi/10.1063/5.0106132/16482657/082102_1_online.pdf

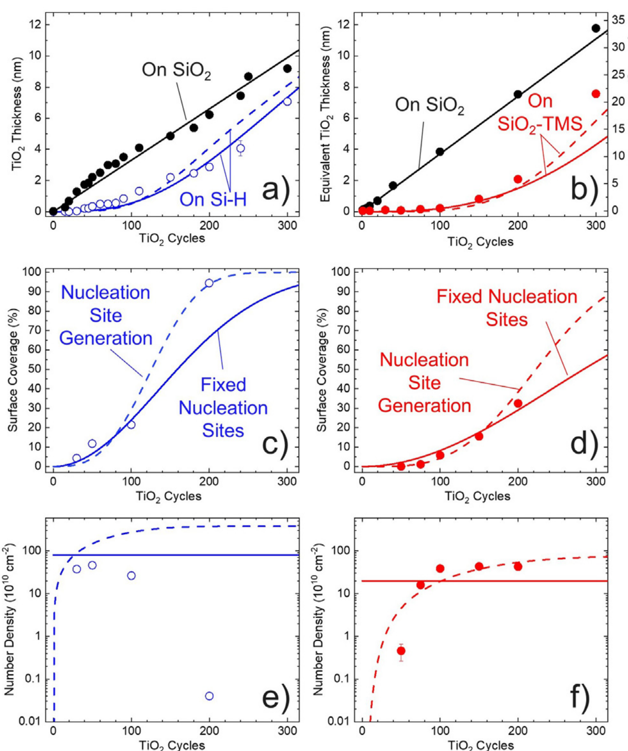

FIG. 3. TiO_2 film thickness and SEM particle analysis data for TiO_2 ALD on Si-H (left column) and SiO_2-TMS (right column) showing (a) and (b) film thickness, (c) and (d) surface coverage, and (e) and (f) number density. Circles represent experimental data on SiO_2 (black), Si-H (blue), and SiO_2-TMS (red), while lines correspond to the model fit, assuming that nucleation site density is constant (solid lines) and nucleation sites are generated during deposition (dashed lines). In (a), thickness on Si-H is obtained by ellipsometry, and in (b), thickness on SiO_2-TMS is estimated from atomic density from RBS [right y-axis in (b)] and expected density, as described in the text. Two thickness points in (b) at 1 and 10 cycles are similarly obtained using TXRF data. Growth is linear on SiO_2 with $\dot{G} = 0.033$ nm cycle^{-1} and $\dot{G} = 0.037$ nm cycle^{-1} in (a) and (b), respectively. On Si-H [(a), (c), and (e)], the solid line fits correspond to $\hat{N} = 0.008$ nm^{-2}, $\dot{N} = 0$ nm^{-2} cycle^{-1} and the dashed fits are $\hat{N} = 0$ nm^{-2}, $\dot{N} = 0.003$ nm^{-2} cycle^{-1}, and $\tau_d = 0$ cycles. On SiO_2-TMS [(b), (d), and (f)], the solid lines correspond to $\hat{N} = 0.002$ nm^{-2}, $\dot{N} = 0$ nm^{-2} cycle^{-1}, and $\tau_d = 0$ cycles, and the dashed fits are $\hat{N} = 0$ nm^{-2}, $\dot{N} = 0.00006$ nm^{-2} cycle^{-1}, and $\tau_d = 50$ cycles.

observed. At 100 cycles, the solid line in Fig. 3(e) is more reasonable, because the dashed line suggests that the nucleus density would be more than 10× larger than observed.

For the thickness data on SiO_2-TMS in Fig. 3(b), the dashed line fit with $\dot{N} > 0$ shows a better overall fit than the solid line ($\hat{N} > 0$) and both fits are reasonable for surface coverage data in Fig. 3(d). The dashed line for $\dot{N} > 0$ also shows a better fit to the particle density data in Fig. 3(f), particularly between 100 and 200 cycles, whereas the solid line fit ($\hat{N} > 0, \dot{N} = 0$) indicates that the number of nuclei would be less than the number of observed particles.

Considering these results, the data and model fits in Fig. 3 show consistent trends. On the Si-H surface, unwanted TiO_2 nuclei form to a large extent due to $\hat{N} > 0$, nucleation sites (e.g., defects, impurities, or non-passivated sites) present on the starting surface, whereas, on the SiO_2-TMS surface, unwanted nuclei form due to $\dot{N} > 0$, the generation of nucleation sites on the growth surface as the ALD process proceeds. Furthermore, this conclusion is consistent with the trends in particle size distributions in Figs. 1 and 2. On Si-H, the narrow PSDs [Fig. 2(a)] with average radius larger than r_n suggest that nucleation sites are present on the starting surface and growth occurs predominantly on these fixed sites [Scheme 1(a)].[23] Thus, particles are similar in size, and they increase in size with each ALD cycle. On SiO_2-TMS, the broad PSDs [Fig. 2(b)] show a large concentration of small particles, which is consistent with nucleation sites continuously generated during ALD [Scheme 1(b)]. In this case, as ALD proceeds, existing nuclei increase in size, and new nuclei form on generated nucleation sites, resulting in a wide range of particle sizes and a high concentration of smaller particles on newly formed sites. Using this insight, potential strategies for selectivity improvement may be deduced. On Si-H, additional substrate preparation steps may reduce initial defects, while on SiO_2-TMS, a periodic defect mitigation step may reduce the impact of generated nucleation sites.

Generally, the $TiCl_4$ reactant is expected to adsorb and react at surface −OH sites present on both the Si-H and SiO_2-TMS.[6,7,24,25] A primary difference between Si-H and SiO_2-TMS is that on the Si-H surface, any remnant Si-OH sites are readily accessible to incoming $TiCl_4$, whereas on the SiO_2-TMS surface, the relatively large TMS groups can sterically shield underlying Si-OH sites. The presence of −OH groups on SiO_2-TMS is consistent with TXRF and RBS data in Fig. 3(b) showing Ti uptake during the first ALD cycle. Quantitatively, TXRF results show the Ti uptake during the first cycle is 4.3×10^{-2} atoms/nm^2. This value is more than 20× larger than the number of sites obtained from the solid line fit on the SiO_2-TMS surface in Fig. 3 ($\hat{N} = 0.002$ nm^{-1}), indicating that after the first ALD cycle, the reacted Ti sites observed by TXRF are predominantly inactive for growth during the immediately following cycles. Future work should aim to incorporate more TXRF measurements at initial cycle numbers to augment modeling parameters. A possible explanation is that on the SiO_2-TMS surface, the Lewis-acidic $TiCl_4$ can transport past the TMS groups and react at surface −OH sites, but during the subsequent H_2O dose, the hydrophobic TMS layer largely impedes water transport, leading to overall slow initial TiO_2 growth.[12]

We also note that the SiO_2-TMS surface remains stable during the ALD process. When the DMA-TMS dose is repeated after every 50 $TiCl_4/H_2O$ cycles (Figs. S2 and S7), the amount of Ti uptake is similar to that with a single DMA-TMS dose, indicating that the $TiCl_4/H_2O$ does not substantially degrade the TMS-passivating layer.[12] Furthermore, as shown in Fig. S5, increasing the TiO_2 deposition temperature to 300 °C leads to the same PSD shape as observed at 150 °C in Fig. 2. Additionally, increasing the purge time during ALD leads to a decrease in the Ti uptake on SiO_2-TMS (Fig. S6), consistent with growth being promoted by reactant physisorption. We conclude, therefore, that TiO_2 nucleation on SiO_2-TMS is initially impeded due to the methyl ligands which sterically block underlying Si-OH sites and that growth eventually occurs when $TiCl_4$ or H_2O reactants become strongly adsorbed or trapped on the SiO_2-TMS surface creating nucleation sites for direct subsequent growth.

In summary, this work demonstrates an experimental/modeling approach to quantify mechanisms leading to unwanted nucleation during low-temperature ASD, demonstrating that unwanted nucleation depends strongly on the nature of the starting passivated surface.

Downloaded from http://pubs.aip.org/aip/apl/article-pdf/doi/10.1063/5.0106132/16482657/082102_1_online.pdf

Published under an exclusive license by AIP Publishing

On the Si-H surface passivated by surface hydrides, nuclei predominantly grow immediately at nucleation sites present on the passivated surface, whereas on SiO_2 passivated by DMA-TMS, nucleation sites are predominantly generated during the growth process, where the nuclei likely form due to ALD reactants that are adsorbed or kinetically trapped on the SiO_2-TMS surface. This establishes that mechanisms associated with unwanted nucleation during ASD depend on the ASD process and substrate and the insight developed here is expected to lead to improved ASD strategies for advanced applications.

See the supplementary material for data related to XPS, WCA, AFM, and RBS on substrates with multiple DMA-TMS passivation steps and selectivity plots for TiO_2 ASD on Si-H and SiO_2-TMS compared to SiO_2.

This project has received funding from the Electronic Component Systems for European Leadership Joint Undertaking under the Grant Agreement No. 692522. The authors also acknowledge funding from the Semiconductor Research Corporation, Task No. 2974.001. The authors would like to thank Ilse Hoflijk, Thierry Conard, Johan Desmet, and Johan Meersschaut (imec, Belgium) for their discussions involving XPS and RBS characterization and data analysis. Additionally, Jan-Willem Clerix is thanked for his insightful discussions on TiO_2 nucleation mechanisms. This work was performed in part at the Analytical Instrumentation Facility (AIF) at North Carolina State University, which is supported by the State of North Carolina and the National Science Foundation (Award No. ECCS-2025064). The AIF is a member of the North Carolina Research Triangle Nanotechnology Network (RTNN), a site in the National Nanotechnology Coordinated Infrastructure (NNCI).

AUTHOR DECLARATIONS

Conflict of Interest

The authors have no conflicts to disclose.

Author Contributions

Rachel Anna Nye: Conceptualization (equal); Data curation (equal); Investigation (equal); Methodology (equal); Writing – original draft (equal); Writing – review and editing (equal). **Seung Keun Song:** Data curation (equal); Writing – review and editing (supporting). **Kaat Van Dongen:** Conceptualization (supporting); Data curation (supporting); Investigation (supporting); Writing – review and editing (supporting). **Annelies Delabie:** Conceptualization (equal); Funding acquisition (equal); Project administration (equal); Resources (equal); Supervision (equal); Writing – review and editing (equal). **Gregory Parsons:** Conceptualization (equal); Funding acquisition (equal); Project administration (equal); Supervision (equal); Writing – review and editing (equal).

DATA AVAILABILITY

The data that support the findings of this study are available within the article and its supplementary material.

REFERENCES

[1]G. N. Parsons and R. D. Clark, Chem. Mater. **32**, 4920 (2020).
[2]A. J. M. Mackus, A. A. Bol, and W. M. M. Kessels, Nanoscale **6**, 10941 (2014).
[3]A. C. Brummer, A. T. Mohabir, D. Aziz, M. A. Filler, and E. M. Vogel, Appl. Phys. Lett. **119**, 142901 (2021).
[4]T. G. Pattison, A. E. Hess, N. Arellano, N. Lanzillo, S. Nguyen, H. Bui, C. Rettner, H. Truong, A. Friz, T. Topuria, A. Fong, B. Hughes, A. T. Tek, A. DeSilva, R. D. Miller, G. G. Qiao, and R. J. Wojtecki, ACS Nano **14**, 4276 (2020).
[5]J.-S. Kim and G. N. Parsons, Chem. Mater. **33**, 9221 (2021).
[6]S. K. Song, H. Saare, and G. N. Parsons, Chem. Mater. **31**, 4793 (2019).
[7]J. Soethoudt, S. Crahaij, T. Conard, and A. Delabie, J. Mater. Chem. C **7**, 11911 (2019).
[8]G. Y. Fang, L. N. Xu, Y. Q. Cao, L. G. Wang, D. Wu, and A. D. Li, Chem. Commun. **51**, 1341 (2015).
[9]Y. Du, X. Du, and S. M. George, J. Phys. Chem. C **111**, 219 (2007).
[10]D. H. Kim, S. Bin Baek, and Y. C. Kim, Appl. Surf. Sci. **258**, 225 (2011).
[11]M. L. Hair and W. Hertl, J. Phys. Chem. **73**, 2372 (1969).
[12]J. Soethoudt, Y. Tomczak, B. Meynaerts, B. T. Chan, and A. Delabie, J. Phys. Chem. C **124**, 7163 (2020).
[13]E. Stevens, Y. Tomczak, B. T. Chan, A. Sanchez, G. N. Parsons, A. Delabie, and K. Leuven, Chem. Mater. **30**, 3223 (2018).
[14]G. N. Parsons, J. Vac. Sci. Technol. A **37**, 020911 (2019).
[15]J. Soethoudt, H. Hody, V. Spampinato, A. Franquet, B. Briggs, B. T. Chan, and A. Delabie, Adv. Mater. Interfaces **6**, 1900896 (2019).
[16]J. Soethoudt, F. Grillo, E. A. Marques, J. R. van Ommen, Y. Tomczak, L. Nyns, S. Van Elshocht, and A. Delabie, Adv. Mater. Interfaces **5**, 1800870 (2018).
[17]H. Saare, S. K. Song, J.-S. Kim, and G. N. Parsons, J. Appl. Phys. **128**, 105302 (2020).
[18]S. E. Atanasov, B. Kalanyan, and G. N. Parsons, J. Vac. Sci. Technol. A **34**, 01A148 (2016).
[19]R. A. Nye, K. Van Dongen, H. Oka, H. Furutani, G. Parsons, D. De Simone, and A. Delabie, Proc. SPIE **12055**, 120550C (2022).
[20]R. A. Nye, S. Wang, S. Uhlenbrock, J. A. I. Smythe, and G. N. Parsons, Dalton Trans. **51**, 1838 (2022).
[21]H. B. R. Lee, M. N. Mullings, X. Jiang, B. M. Clemens, and S. F. Bent, Chem. Mater. **24**, 4051 (2012).
[22]K. Van Dongen, R. Nye, D. De Simone, and A. Delabie, in AVS ALD (2021).
[23]R. L. Puurunen, W. Vandervorst, W. F. A. Besling, O. Richard, H. Bender, T. Conard, C. Zhao, A. Delabie, M. Caymax, S. De Gendt, M. Heyns, M. M. Viitanen, M. De Ridder, H. H. Brongersma, Y. Tamminga, T. Dao, T. De Win, M. Verheijen, M. Kaiser, and M. Tuominen, J. Appl. Phys. **96**, 4878 (2004).
[24]M. M. Frank, Y. J. Chabal, M. L. Green, A. Delabie, B. Brijs, G. D. Wilk, M. Y. Ho, E. B. O. Da Rosa, I. J. R. Baumvol, and F. C. Stedlle, Appl. Phys. Lett. **83**, 740 (2003).
[25]M. M. Frank, Y. J. Chabal, and G. D. Wilk, Appl. Phys. Lett. **82**, 4758 (2003).

Downloaded from http://pubs.aip.org/aip/apl/article-pdf/doi/10.1063/5.0106132/16482657/082102_1_online.pdf

Published under an exclusive license by AIP Publishing